

Article

Distributed Coordination Control Based on State-of-Charge for Bidirectional Power Converters in a Hybrid AC/DC Microgrid

Zeyan Lv, Yanghong Xia , Junwei Chai, Miao Yu *  and Wei Wei

College of Electrical Engineering, Zhejiang University, Hangzhou 310027, China; lvzeyan@zju.edu.cn (Z.L.); royxiayh@126.com (Y.X.); chajunwei_bit@163.com (J.C.); wwei@zju.edu.cn (W.W.)

* Correspondence: zjuyumiao@zju.edu.cn

Received: 20 March 2018; Accepted: 18 April 2018; Published: 20 April 2018



Abstract: This paper proposes a distributed coordination control for multiple bidirectional power converters (BPCs) in a hybrid AC/DC microgrid with consideration of state-of-charge (SOC) of storages. The researched hybrid AC/DC microgrid is composed of both AC and DC subgrids connected by multiple parallel BPCs. In the literature, the storages of a hybrid microgrid are considered to allocate in only the AC subgrid or DC subgrid, which reduces the reliability of the whole system, especially during the islanded mode. Besides, the SOC management has not been considered in BPCs' operating strategy. This paper considers a hybrid microgrid topology which has energy storages in both AC side and DC side. This ensures the reliability while increasing the complexity of the control strategy at the same time. Further, a distributed coordination control method for multiple BPCs based on SOC was proposed to enhance the reliability of hybrid microgrid. Finally, the performance of the proposed control methods was verified by real-time hardware-in-loop (HIL) tests.

Keywords: hybrid AC/DC microgrid; parallel bidirectional power converters (BPCs); distributed control; power sharing; SOC management

1. Introduction

Microgrid has become a widely accepted concept due to its high reliability and high flexibility. The operating environment of microgrid is more complex than normal distribution network because there are not only fluctuating loads but also intermittent distributed generators. Therefore, the research on the microgrid control method is highly desirable to ensure the safe and stable operation of the microgrid [1–3]. In general, a microgrid operates in grid-connected mode or in islanded mode according to the actual demand [4]. Microgrids that operate in grid-connected mode consider more about optimal management problems and optimal dispatching strategies because the voltage support and power balance can be realized by the utility grid. Microgrids that operate in islanded mode should first ensure the stable operation. Researchers have done a lot of work in isolated microgrid's stable operation [5,6]. The strategy this paper proposes has both grid-connected mode and islanded mode.

Considering the inherent characteristics, the DC load is far more than the AC load, but, because the traditional power grid is still an AC network, the construction of pure DC microgrid is relatively difficult. Thus, the hybrid AC/DC microgrid is put forward recently to facilitate the integration of DC microgrid. A typical hybrid AC/DC microgrid has an AC subgrid and a DC subgrid connected by bidirectional power converters (BPCs). In general, distributed generators such as PV cell and wind power are volatile. To suppress power fluctuations and to maintain the bus voltage in the islanded condition, an energy storage system is necessary in the microgrid [7,8].

For hybrid AC/DC microgrids, the energy storage system is usually set on either AC side or DC side. However, the topology which only has storage on one side of the hybrid microgrid may have obvious defects. When the hybrid microgrid operates in the islanded mode, the BPCs must work as voltage sources to maintain the bus voltage for the subgrid that does not have storage system. When the storage system goes wrong, the whole microgrid breaks down. Besides, in such microgrid system, the AC subgrid and DC subgrid can never work alone because of mutual support and BPCs are desired to always participate in the power management. However, in practice, AC subgrid or DC subgrid may be asked to work alone at times. To meet the demand of power distribution reliability, this paper studied a new topology, which has energy storage systems on both sides of the AC/DC microgrid. All storages operate in voltage mode when the microgrid loses connection with the utility. Each subgrid can work as an independent system and they can also operate in coordination.

In this architecture, the SOC management must be considered in the coordination control. Otherwise, the unilateral microgrid may break down because of over-rapid battery discharging in one side. A good solution is to incorporate the SOC management into BPCs' control strategy, as adjusting the output power of BPCs will change the storage's output and consequently control the SOC of storages in both AC side and DC side. Nevertheless, the status of SOC is rarely considered in the control strategy of BPCs. In conventional AC/DC microgrids, the multiple BPCs are used mainly to manage the power and to achieve interaction between subgrids. The methods which are designed to balance the power of each subgrid have been proposed in [9–11]. Wang et al. [12] created a three-port hybrid microgrid to achieve the power sharing. Xiao et al. [13] proposed an improved method to reduce the power sharing deviation. Some researchers realized the power interaction by establishing the relationship between frequency and DC bus voltage [14–16].

On the other hand, the control of SOC is usually realized by the storage's interface converter at present. For a single storage system, it does not have another operation mode except voltage source in the islanded mode. However, single storage system still has over discharging and over charging problems. Cutting off some loads may be the only way to solve the over discharging problem. Thus, studies pay more attention to the overcharging. When the DGs' output power is more than load's power by a significant margin for a long time, the storage will have the overcharging problem. Gu et al. [17] designed a distributed control strategy which makes the overcharged storage exit voltage source mode and keeps one PV converter to regulate the bus voltage at the same time by changing PV converters' operating mode from current source to voltage source. Sun et al. [18] presented a mechanism that PV converters exit one after another by sampling differences of bus voltage. In addition, if the communication technology allows, the centralized secondary control is a good solution for SOC management problems [19]. For those systems that have multiple storage systems in a subgrid, droop control is an effective way to share the active power [20]. Changing the droop coefficient is a good way to balance the SOC of the multiple storage systems [21]. Karimi et al. [22] proposed a decentralized SOC management strategy which regards the PV and the battery as a whole. Hosseinzadeh and Salmasi [23] focused on the development of a supervisory control scheme for maintaining SOC of battery banks. However, the coordinated SOC control for AC/DC hybrid microgrids with multiple storages in both subgrids has not been investigated.

Hence, this paper puts forward a SOC based distributed coordination control for multiple BPCs, in which BPCs can balance SOC of storages in both AC subgrid and DC subgrid to avoid output power of storage exceeding the maximum. The rest of this paper is organized as follows. In Section 2, the mathematical model of the BPC is proposed and the inner loop control strategy of BPCs which can suppress the circulating currents effectively is introduced. In Section 3, the outer loop control methods in both islanded mode and grid-connected mode are proposed. In Section 4, the small signal model of the hybrid AC/DC microgrid is established to analyse the stability of the system. In Section 5, the HIL test results have been shown to verify the effect of the proposed method. The conclusion is made in Section 6.

2. Inner Loop Control

As shown in Figure 1, the researched hybrid AC/DC microgrid is composed of an AC subgrid and a DC subgrid. The control strategies for multiple BPCs in this paper can be divided into two layers. The inner loop control is mainly to control the output parameters of the BPC to follow the references generated by the outer loop control. It is also designed to suppress the circulating currents between the BPCs. The outer loop of BPCs balances SOC of storages in both AC subgrid and DC subgrid to avoid output power of storage exceeding the maximum.

Other devices in the hybrid AC/DC microgrid still use conventional methods during operation. Distributed generators such as photovoltaic and wind turbines always operate in maximum power tracking mode. Storages on both sides operate in constant power mode in the grid-connected mode. In the islanded mode, the storage on AC side is controlled by AC droop to support AC subgrid voltage and frequency. At the same time, the storage on DC side is controlled by DC droop to support DC subgrid voltage.

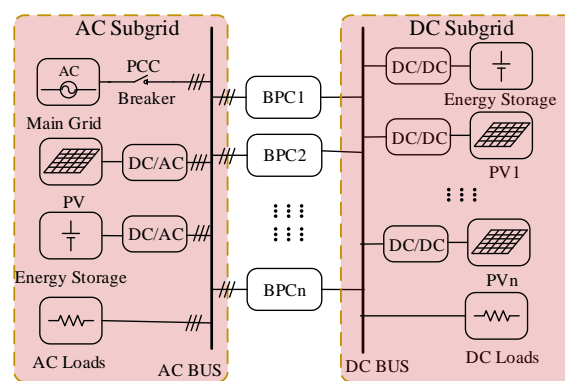


Figure 1. Hybrid microgrid topology with energy storages on both sides.

The structure of a BPC is shown in Figure 2. According to Kirchhoff’s voltage law, the loop equations of BPC can be described as

$$L \frac{di_{Lk}}{dt} + ri_{Lk} = v_k - V_{dc}s, \tag{1}$$

where $k = a, b, c$, L is the filter inductance, r is the parasitic resistance of L , s is switch function, v_k is the phase voltage of AC Bus, i_{Lk} is the current of L and we suppose that the direction of i_{Lk} from AC side to DC side is positive.

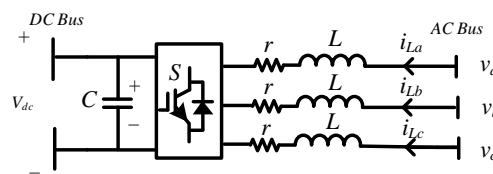


Figure 2. Topology of bidirectional power converter.

By Clark and Park coordinate transformation, the transformation from a - b - c to d - q -0 is

$$\begin{bmatrix} x_d \\ x_q \\ x_0 \end{bmatrix} = \frac{2}{3} \begin{bmatrix} \cos \theta & \cos(\theta - 2\pi/3) & \cos(\theta + 2\pi/3) \\ \sin \theta & \sin(\theta + 2\pi/3) & \sin(\theta - 2\pi/3) \\ 1/2 & 1/2 & 1/2 \end{bmatrix} \begin{bmatrix} x_a \\ x_b \\ x_c \end{bmatrix}, \tag{2}$$

where θ is the rotation angle as shown in Figure 3.

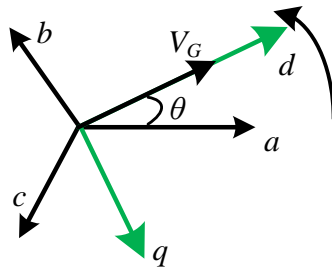


Figure 3. Coordinate transformation.

Ignoring the loss of switch tubes and parasitic resistance, the average model of a single BPC could be expressed as

$$\begin{cases} L \frac{di_d}{dt} = -ri_d + i_q\omega L + V_G - v_d \\ L \frac{di_q}{dt} = -ri_q - i_d\omega L - v_q \\ L \frac{di_0}{dt} = -ri_0 - v_0 \\ \frac{1}{2}C \frac{dv_{dc}^2}{dt} = \frac{3}{2}V_G i_d - P_{dc} \end{cases}, \tag{3}$$

where V_G is the amplitude of AC bus voltage, v_{dc} is the dc port voltage of BPC, P_{dc} is the output power on the DC side of BPC, and C is the capacitance of BPC’s DC side.

According to the Equation (3), v_{dc}^2 and i_d can be regarded as a linear relationship while ignoring P_{dc} . Therefore, some authors put forward a new control strategy which is established based on v_{dc}^2 rather than v_{dc} [24]. Furthermore, they used compensation decoupling control to decouple the i_d and i_q .

For a single BPC, the decoupled control of i_d and i_q is good enough for active power and reactive power control. However, circulating currents occur in a multiple BPC system because of different switch states of the BPCs [25]. The strategy which can solve the circulating currents problem is to add a 0-axis control [26].

In conclusion, the inner loop control is designed as shown in Figure 4. The reference of d -axes is $(v_{dc}^{ref})^2$ and the references of q -axes and 0-axis are both current signals. The controller of 0-axis is intended to restrain the circulating current. Set $i_0^{ref} = 0$. $G1, G2, G3$ are proportional integral (PI) controllers.

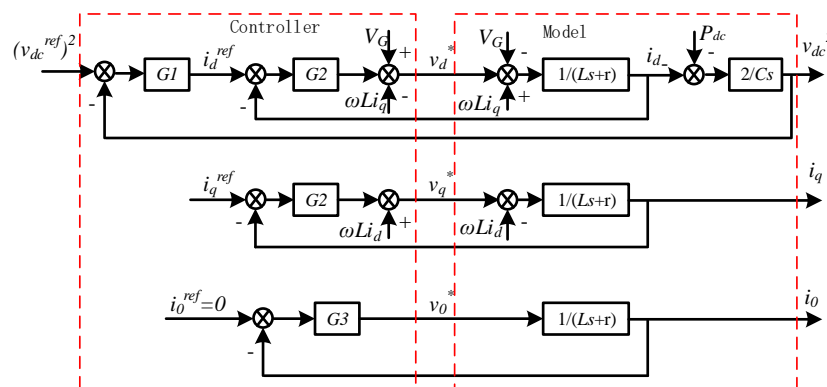


Figure 4. Inner loop control strategy.

3. Outer Loop Control

The hybrid microgrid may operate in grid-connected mode or islanded mode in practice, and the storage systems work with different strategies during these two situations. To meet the requirement of stable operation, the outer loop control of BPCs can support DC side bus voltage in the grid-connected mode and can manage SOC to avoid excessive power output of the storages in the islanded mode.

3.1. Grid-Connected Mode

In this mode, the storage system on both AC side and DC side will charge in constant power mode or just in float mode. In this case, the utility grid will support the voltage and frequency of AC subgrid bus. The BPCs play the role of DC subgrid bus voltage sources by DC droop control. The active power among different BPCs should be equally shared. The equation of DC droop control is

$$V_{dc,n}^{ref} = V_{dc,n}^* - mI_{dc,n}, \tag{4}$$

where n denotes n -th BPC, and $V_{dc,n}^*$, m , and $I_{dc,n}$ represent the rated DC voltage, DC droop control coefficient and real-time DC side current of n -th BPC, respectively.

To share the reactive power on the AC side, the AC reactive power droop control is adopted as

$$Q_n^{ref} = Q_n^* - k_d(V_n - V_n^*), \tag{5}$$

where Q_n^* is the rated output reactive power of n -th BPC, k_d is the coefficient of AC droop control, V_n is the real-time AC voltage and V_n^* is the rated AC voltage of the n -th BPC. Use $i_q^{ref} = \frac{2}{3} \times \frac{Q_n^{ref}}{V_n}$ to get the reference of inner loop i_q^{ref} .

3.2. Islanded Mode

In the islanded mode, the storage on AC side will change into AC droop mode and work as a voltage source, and thus the AC bus voltage amplitude and frequency can be controlled by the storage. Meanwhile, the storage on DC side will start to support the DC bus voltage. Under this circumstance, both DC bus and AC bus can be supported independently and the output power of storage is passive. Therefore, the BPCs can work as power sources and achieve the SOC management and storage's maximum output limit by transferring the active power from one side to another.

The reactive power sharing method is the same as the grid-connected mode, while the active power control strategy with consideration of SOC can be modified as shown in Figure 5. BPCs get the SOC of storages on both AC side and DC side and calculate the real-time active power reference by SOC loop. The SOC information of each storage needs to be transferred by communication lines in this algorithm. There has been a lot of progress on SOC estimation [27–31]. The SOC estimation method this paper adopted can be expressed as

$$SOC_i = SOC_{i,t=0} - \frac{1}{C_e} \int p_{in,i} dt, \tag{6}$$

where i represents the i -th storage system, and $SOC_{i,t=0}$, C_e , and $p_{in,i}$ are initial SOC at $t = 0$, power capacity and input power, respectively.

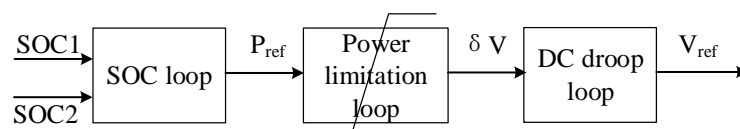


Figure 5. Outer loop control block diagram.

The SOC loop and power limitation loop finally output δV , which is added to DC droop formula to get V_{ref} . The modified DC droop control can be expressed as

$$V_{dc,n}^{ref} = V_{dc,n}^* - mI_{dc,n} + \delta V. \quad (7)$$

The SOC loop and power limitation loop are introduced in detail in the following.

3.2.1. SOC Loop

The SOC loop can be described as in Figure 6. This loop decides the real-time active power transferred by BPCs from one subgrid to another. When the microgrid system operates in islanded mode, we expect that each SOC of storage has a healthy state. In general, SOC of storage maintained around 50% is optimal. Once the SOC is lower than 20% or higher than 80%, some strategies should be implemented to limit the storage's discharging or charging power.

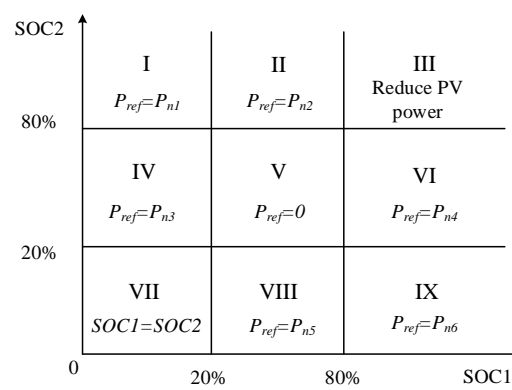


Figure 6. Quadrantal diagram of outer loop control.

According to these rules, the proposed strategy divides the SOC states into nine quadrants. When the two SOC's are both between 20% and 80% (Quadrant 5), the storages in both AC side and DC side are in normal conditions. Thus, BPCs will not deal with the active power and the output power reference of BPCs will be zero. When the two SOC's both exceed 80% (Quadrant 3), BPCs will not be able to regulate active power and the output of DGs should be reduced to restrain the storages from charging.

Once $SOC1 < 20\%$ and $SOC2 < 20\%$ (Quadrant 7), the SOC's of storages on both AC side and DC side are at a low level, and we hope that the SOC's on both sides can decline synchronously, so that the whole hybrid microgrid can stay longer before the DGs' output power increases. The strategy is to keep the SOC's on both sides equal, that is, $SOC1 = SOC2$. A PI controller has been used to get the P_{ref} . Thus, the equation of Quadrant 7 can be expressed as

$$P_{ref} = \left(K_p + \frac{K_i}{s} \right) \cdot (SOC1 - SOC2), \quad (8)$$

where $SOC1$ is the AC side storage's state of charge and $SOC2$ is the DC side storage's state of charge. Once the SOC state goes into Quadrant 7 and the storages start to charge, the SOC's of two storages will increase synchronously.

When the value of SOC is in Quadrants 2, 4, 6 and 8, one side of SOC in the hybrid microgrid is not in normal conditions. Thus, the strategy uses a proportional algorithm to make the trend of BPCs' output power be opposite to that of SOC. If the SOC changes further away from the boundary value, the active power transferred by BPCs will increase. In Quadrants 1 and 9, SOC of storages on both AC side and DC side are not in good conditions and we need to choose one SOC as a reference. Thus, we should compare the difference between the current SOC and the quadrant boundaries (80% or 20%)

and then use the aforementioned proportional algorithm to get P_{ref} based on the larger difference. The detailed expressions in these six quadrants of Figure 6 are

$$\begin{cases} P_{n1} = -k_l \cdot (SOC_m) \\ P_{n2} = -k_l \cdot (SOC2 - 0.8) \\ P_{n3} = k_l \cdot (SOC1 - 0.2) \\ P_{n4} = k_l \cdot (SOC1 - 0.8) \\ P_{n5} = -k_l \cdot (SOC2 - 0.2) \\ P_{n6} = k_l \cdot (SOC_n) \end{cases}, \quad (9)$$

where k_l is a proportion coefficient of the method, and $k_l = 5P_{max}$, $SOC_m = \max(\text{abs}(SOC1 - 0.2), \text{abs}(SOC2 - 0.8))$, $SOC_n = \max(\text{abs}(SOC1 - 0.8), \text{abs}(SOC2 - 0.2))$. P_{max} is maximum active power of BPCs.

The parameter k_l makes P_{ref} change from 0 to P_{max} proportionally. Once either SOC reaches the upper boundary (100%) or lower boundary (0%), P_{ref} will reach the maximum. When at the border of the quadrant, the result of SOC loop will not change suddenly. Thus, the proportion control can realize the smooth transition between the various quadrants. A detailed quadrant switch will be illustrated later by Case 3 in Section 5.

3.2.2. Power Limitation Loop

In the islanded mode, the active power of BPCs should be limited to avoid storages exceeding the maximum output power. Thus, this loop is designed to limit the P_{ref} from SOC loop and output δV for Equation (7). According to the characteristic of hybrid AC/DC microgrid, the load on DC side should be powered by BPCs in grid-connected mode, so

$$\sum P_{BPCn} = P_{str2,rate}, \quad (10)$$

where $P_{str2,rate}$ is the rated active power of storage on DC side, and P_{BPCn} is the maximum active power of n -th BPC. Suppose that the direction of active power injecting into AC side is positive and the direction of discharging is positive. The maximum active power of storage on DC side is equal with the maximum active power of storage on AC side. Then,

$$P_{ref} - \sum P_{BPCn} < \min((P_{str2,rate} - P_{str2}), (P_{str1,rate} + P_{str1})), \quad (11)$$

$$P_{ref} - \sum P_{BPCn} > \max((-P_{str2,rate} - P_{str2}), (-P_{str1,rate} + P_{str1})), \quad (12)$$

where P_{BPCn} is n -th BPC's rated output active power; P_{str1} is storage's real-time active power on AC side; P_{str2} is storage's real-time active power on DC side; $P_{str1,rate}$ is storage's rated active power on AC side; and $P_{str2,rate}$ is storage's rated active power on DC side.

The simplified structure of BPC on DC side is shown in Figure 7, where r is the output impedance. The output of BPCs can be expressed as $P_{ref} = V_{dc} \cdot I_{dc}$, and $I_{dc} = (V_{ref} + \delta V - V_{dc})/r$. δV can be derived from $\delta V = P_{ref} \cdot r/V_{dc} + V_{dc} - V_{ref}$ and $V_{ref} = V_{dc}$ when system access steady state. Thus, δV is defined as $\delta V = P_{ref} \cdot r/V_{dc}$.

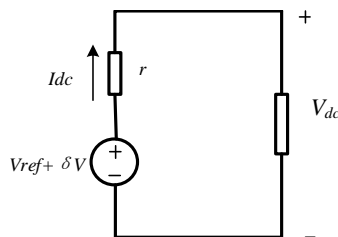


Figure 7. DC side equivalent diagram.

4. Stability Analysis of Hybrid AC/DC Microgrid

In this section, the stability of outer loop control proposed in Section 3.2 is studied. Analysing the SOC control loop proposed in Figure 6, the control method in each quadrant can be achieved by BPCs. When the BPCs operate in Quadrants 1, 2, 4, 6, 8 and 9, they can be regarded as constant power source and the stability of constant power source in microgrid has already been analysed. Therefore, this section concentrates mainly on the stability of strategy in Quadrant 7.

To simplify the model of the microgrid system, the distributed generators on AC side and DC side operate in MPPT mode and can be considered as power sources. Thus, the output power of AC DGs and DC DGs can be expressed as $P_{pv,ac} + Q_{pv,ac}$ and $P_{pv,dc}$, respectively. Similarly, the load on AC side can be expressed as $P_{load,ac} + Q_{load,ac}$ and the load on DC side can be adopted as $P_{load,dc}$ ignoring the small voltage deviation of DC bus. Thus, the simplified model is shown in Figure 8.

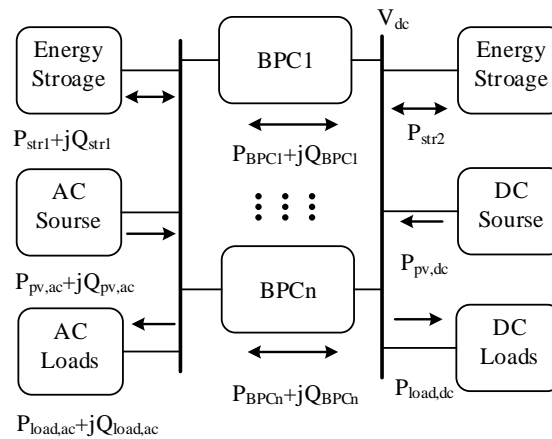


Figure 8. Simplified hybrid AC/DC microgrid.

According to Equation (6), the SOC_{dev} can be expressed as

$$SOC_{dev} = \frac{P_{str2}}{C_e S} - \frac{P_{str1}}{C_e S} + SOC_{1,t=0} - SOC_{2,t=0}, \quad (13)$$

where $SOC_{dev} = SOC1 - SOC2$, P_{str1} is the active power of storage system on AC side and P_{str2} is the active power of storage system on DC side.

Using small-signal model to linearize the expression, we can get

$$\Delta \dot{SOC}_{dev} = \frac{\Delta P_{str1} - \Delta P_{str2}}{C_e}, \quad (14)$$

The input of the power limitation loop can be expressed as

$$P_{ref} = \left(K_p + \frac{K_i}{s} \right) SOC_{dev}. \quad (15)$$

Linearizing the expression, we have

$$\Delta \dot{P}_{ref} = K_p \Delta SOC_{dev} + K_i \Delta SOC_{dev}. \quad (16)$$

As for the BPC, the inner loop transfer function can be simplified as “1”, which means that $(V_{dc}^{ref})^2 = V_{dc}^2$, $i_q^{ref} = i_q$ and $i_0^{ref} = i_0$. Thus, the n -th BPC's output DC voltage and output active power can be expressed as

$$V_{dc,n} = V_{dc,n}^{ref} - m I_{dc,n} + a P_{ref}, \quad (17)$$

$$P_{BPC,k} = V_{dc,n} I_{dc,n}, \quad (18)$$

where $a = r/V_{dc}$.

Ignoring the line loss, the equation of power balance on AC side and DC side can be expressed as

$$P_{pv,ac} - P_{load,ac} + P_{str1} = \sum_{k=1}^n P_{BPC,k}, \quad (19)$$

$$P_{pv,dc} - P_{load,dc} + P_{str2} = -\sum_{k=1}^n P_{BPC,k}. \quad (20)$$

Linearizing Equations (18)–(20), we can get

$$\Delta P_{BPC,k} = \Delta V_{dc,n} I_{dc,n} + \Delta I_{dc,n} V_{dc,n}, \quad (21)$$

$$\Delta P_{str1} = \sum_{k=1}^n \Delta P_{BPC,k}, \quad (22)$$

$$\Delta P_{str2} = -\sum_{k=1}^n \Delta P_{BPC,k}, \quad (23)$$

where $I_{dc,n}$ and $V_{dc,n}$ are the steady DC current and steady DC voltage of n -th BPC, respectively. Substituting Equations (21)–(23) into Equation (14), we have

$$\Delta SOC_{dev} = \Delta P_{ref} \frac{2a \sum (I_{dc,n})(-V_{dc})}{C_e \sum (mI_{dc,n} - V_{dc,n} - V_{dc})}. \quad (24)$$

Above all, the small signal mode of the simplified hybrid AC/DC microgrid can be obtained as

$$\dot{X} = AX, \quad (25)$$

$$X = \begin{bmatrix} \Delta SOC_{dev} \\ \Delta P_{ref} \end{bmatrix}, \quad (26)$$

$$A = \begin{bmatrix} 0 & Y \\ K_i & K_p Y \end{bmatrix}, \quad (27)$$

$$Y = \frac{2a \sum (I_{dc,n})(-V_{dc})}{C_e \sum (mI_{dc,n} - V_{dc,n} - V_{dc})}. \quad (28)$$

For a two-parallel-BPC hybrid microgrid whose detailed parameters are given in Table 1, the dominant poles locus of A as K_p from 0.1 to 20 and as m from 0.1 to 100 are shown in Figures 9 and 10. It can be seen that the dominant poles moves toward the zero imaginary axis finally with the K_p and m increasing. Thus, the system will be unstable if the K_p and m are too large.

Table 1. System simulation parameters.

Microgrid Parameters	Rated Values
AC bus voltage V/f	380 V/50 Hz
DC bus voltage V_{dc}	600 V
AC load	30 kW+5 kVar
DC load	36 kW
DC PV output power	80 kWp
AC PV output power	40 kWp
AC line impedance	0.001 Ω , 1.2 mH
DC line resistance	0.001 Ω
Storage capacity	100 W·h

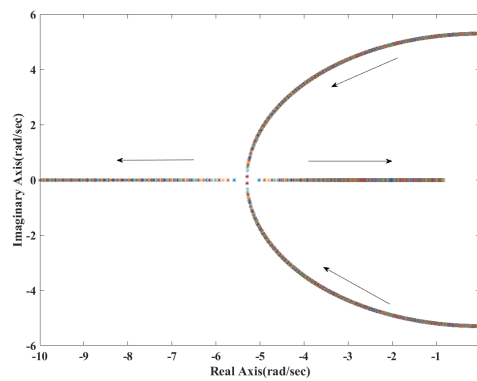


Figure 9. $m = 0.4$ and K_p increases from 0.1 to 20.

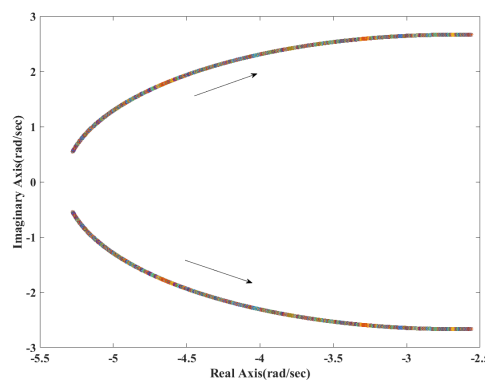


Figure 10. $K_p = 6$ and m increases from 0.1 to 100.

5. Hardware-in-Loop Tests

To verify the proposed distributed coordination control strategy, a simulated hybrid microgrid model was set up in RT/LAB. As shown in Figure 11a, the hybrid microgrid included AC subgrid, DC subgrid and BPCs. The AC subgrid had an AC storage system, a distributed generator (PV) and an AC load. The AC bus was connected to the utility grid, which was established by infinity power source. The DC subgrid consisted of a DC storage system, a distributed generator (PV) and a DC load. The AC subgrid and DC subgrid were connected by two parallel BPCs. The detailed parameters are shown in Table 1. For the BPCs, the main parameters are as follow: $m_1 = m_2 = 0.4 \text{ V/A}$, $V_{dc,1}^* = V_{dc,2}^* = 600 \text{ V}$, $Q_1^* = Q_2^* = 2 \text{ kVar}$, $V_1^* = V_2^* = 311 \text{ V}$, $k_{d1} = k_{d2} = 500 \text{ Var/V}$, $K_{p,1} = K_{p,2} = 6$, and $K_{i,1} = K_{i,2} = 16$. To shorten the simulation time, this paper adopts a storage model that has a normal rated output power but a small battery capacity.

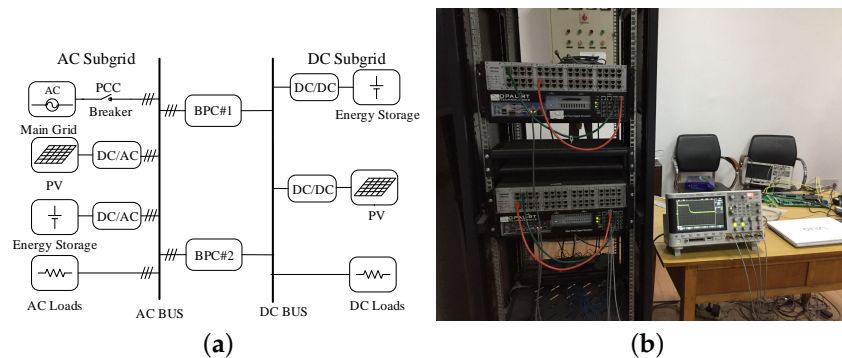


Figure 11. (a) Hardware-in-loop tests topology; and (b) Hardware-in-Loop (HIL) test facility.

Case 1: This case concentrates on the mode switch. The proposed hybrid microgrid control method can achieve grid-connected operation and islanded operation. Figure 12a shows the output power of BPCs, DC bus voltage and AC bus voltage during the mode switch. The two storages' SOCs in this test are normal. The hybrid microgrid starts from grid-connected mode (Stage I). At the start of test, the system goes into steady state and the storage system works in floating charging mode. The AC bus voltage and frequency are supported by utility grid. DC voltage is supported by BPCs. The output of one BPC is about 18 kW. Then, the system switches into smooth transition (Stage II). The system disconnects from utility grid at the end of Stage I and storage system operates as a voltage source at the same time. BPCs do not change mode during the smooth transition. From the beginning of Stage II, two BPCs and the DC storage share the DC side power together. However, the power that storage shares is more than BPCs. There is a voltage deviation in DC voltage bus shown in Figure 12b because the droop control causes the voltage lifting when the output current reduces. The smooth transition completes at the end of Stage II, and the system goes into islanded mode (Stage III). The output of BPCs is zero when two storages' SOCs are normal. As shown in Figure 12c, during the mode switching, the AC voltage will have a small fluctuation. The frequency changes a little, and the amplitude of the AC bus voltage has a deviation because of using AC reactive power droop control method. Besides, a contrast test was done to show the advantage of smooth transition strategy. It can be seen in Figure 12d that the DC bus voltage drops about 40 V if the mode switching does not have smooth transition strategy. Thus, the smooth transition does well in supporting the DC bus voltage.

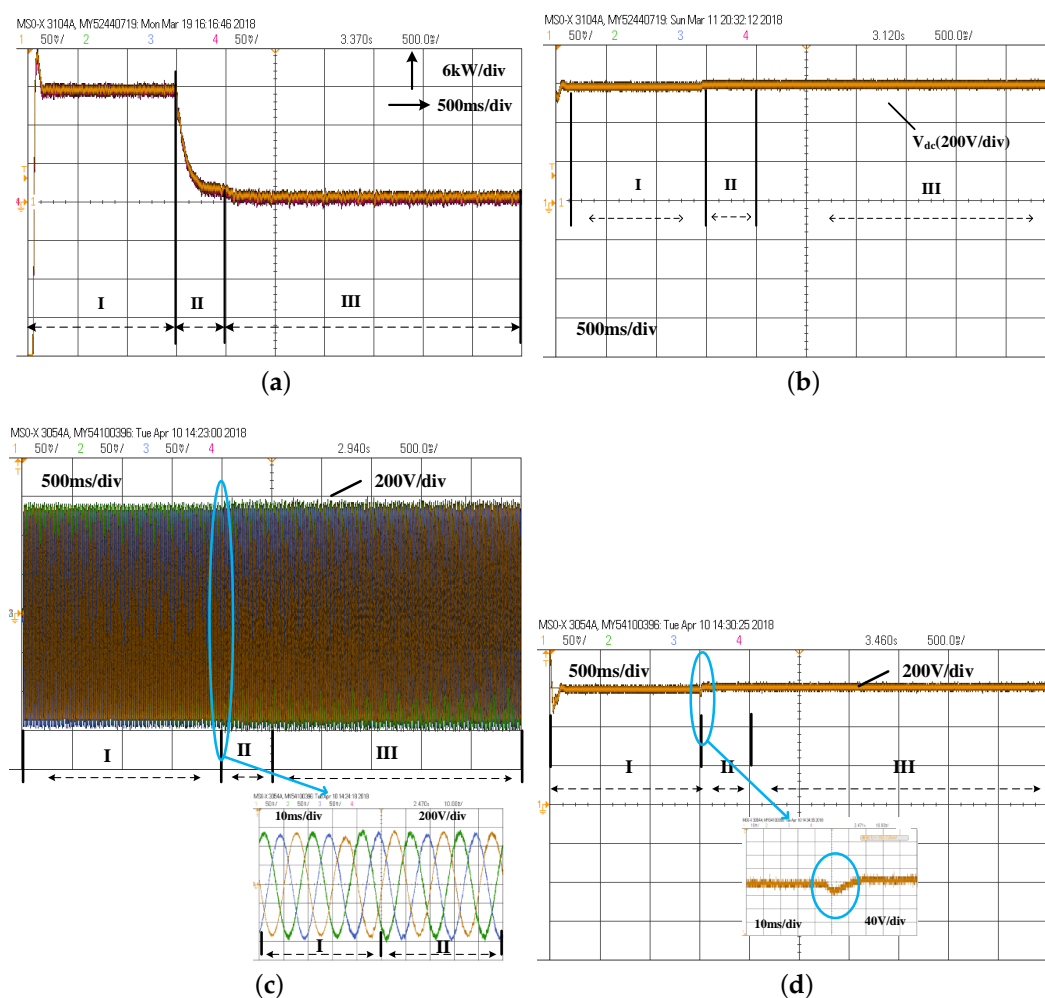


Figure 12. Test results of Case 1: (a) output power of BPCs; (b) DC voltage; (c) AC voltage; and (d) DC voltage in microgrid without smooth transition method.

Case 2: This case is a contrast experiment. A severe operating environment has been assumed to verify that whether the SOC based algorithm this paper proposed will hold out longer than the microgrid system which does not have a SOC management method in islanded mode. The initial SOC is 20%. The PV output in DC subgrid is 37 kW, and the output power of PV on AC side is 0 kW in this case. The system without proposed control strategy is shown in Figure 13b. The AC side does not have other power sources except storage. Thus, the SOC in AC storage reduces quickly. At the same time, the PV output on DC side is larger than the DC load, so the DC storage is charging. The microgrid goes wrong at 2.25 s for the lack of SOC on AC side. The strategy this paper proposed is better in comparison. As shown in Figure 13a, SOC_s on both side declines synchronously after a period of adjustment. The microgrid is still in operation at 4 s. Thus, the microgrid in this method can stay longer in the severe operating environment.

Case 3: This case tests a complete islanded operation. As shown in Figure 6, the outer loop control is symmetrical. Thus, the test of switching between quadrants can be designed, as shown in Figure 14. The result of the test is shown in Figure 15. Both AC load and DC load work in rated parameters and $P_{pv,dc} = 0$ kW, $P_{pv,ac} = 20$ kW at the beginning. The initial SOC_s of storages on AC side and DC side are both 50%. Thus, the test starts at Quadrant 5 and the output of BPCs is 0 at Stage I. The SOC of storage on DC side decreases to 20% first so the algorithm changes to Quadrant 8 at the beginning of Stage II. The output of BPCs increases in proportion at Stage II. The algorithm changes to Quadrant 7 at Stage III because the SOC_s of storages on both AC side and DC side are lower than 20% and the SOC_s of storages begin to decrease synchronously. Then, the output of PV on DC side increases at Stage IV. The SOC_s will increase synchronously because the control method does not change and the SOC_s will be 20% at the end of StageIV. The algorithm changes to Quadrant 4 due to that storage on DC side keeps charging and storage on AC side starts discharging in the absence of BPCs' help. At StageV, SOC₁ will maintain a value slightly below 20% and SOC₂ keeps increasing. Finally, the output of PV on AC side increases and the output of PV on DC side decreases. Nevertheless, the output of BPCs will not change immediately, and according to $P_{BPC1} + P_{BPC2} + P_{load,dc} = P_{pv,dc} + P_{str2}, P_{str1} + P_{load,dc} = P_{pv,ac} + P_{BPC1} + P_{BPC2}, P_{str2}$ increases and P_{str1} reduces. Thus, SOC₂ has a small decline at the beginning of StageVI. However, owing to $P_{pv,dc} > P_{load,dc}$ and $P_{pv,ac} > P_{load,ac}$, the algorithm changes back to Quadrant 5 at StageVI in the end of test. Besides, the output power is well shared among the two BPCs during the whole process.

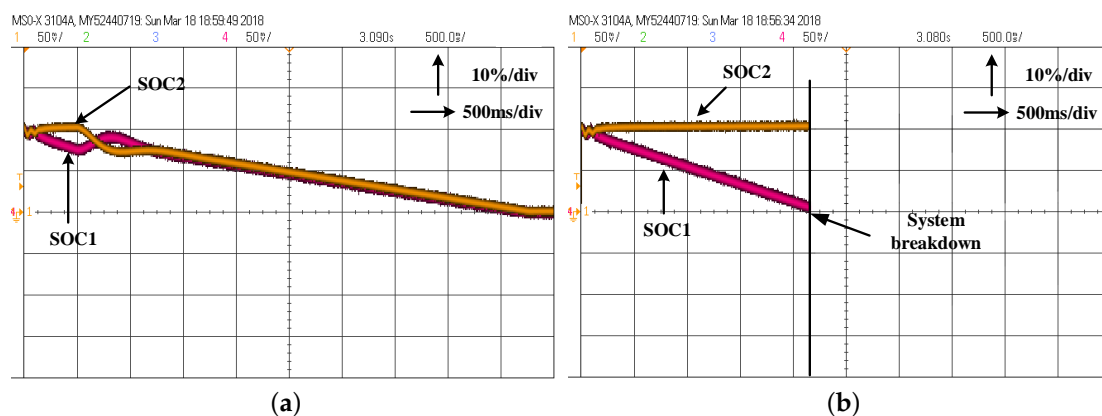


Figure 13. Test results of Case 2: (a) SOC_s of storages when BPCs are controlled by proposed strategy; and (b) SOC_s of storages when BPCs are controlled without proposed strategy.

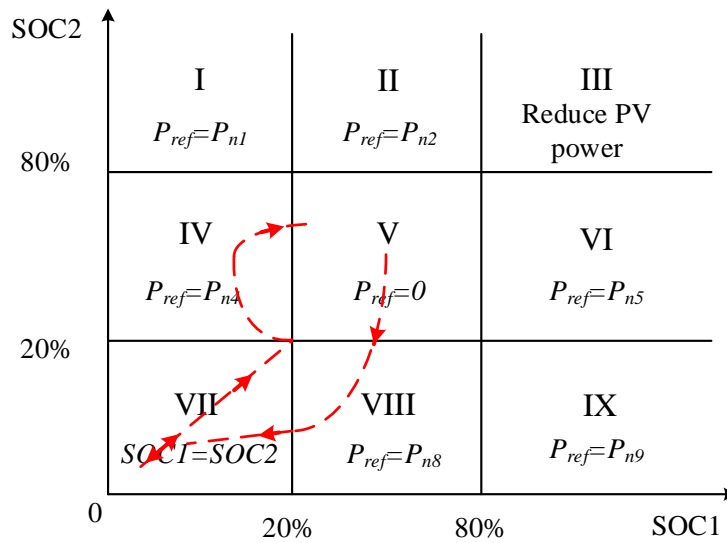


Figure 14. Quadrant switching path of case 3.

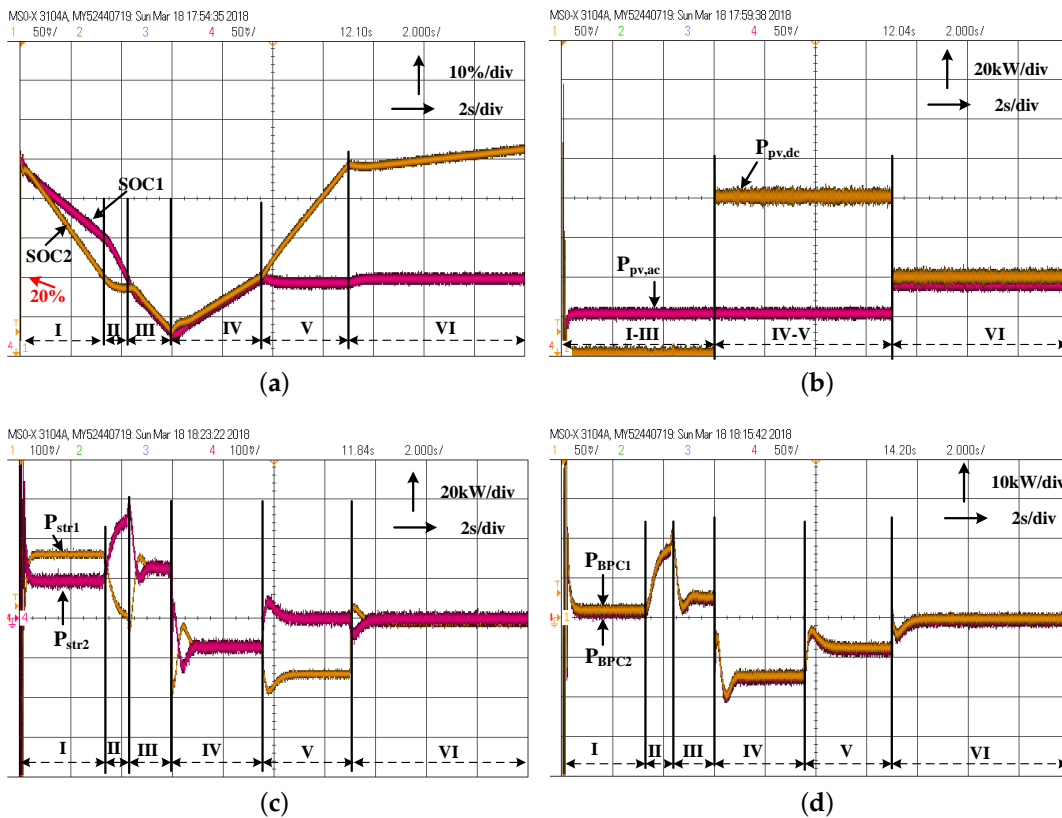


Figure 15. Test results of Case 3: (a) SOCs of the storage on AC side and DC side; (b) output power of PV; (c) output power of AC storage and DC storage; and (d) output power of BPCs.

6. Conclusions

In this paper, a SOC based distributed coordination control method is proposed for parallel BPCs in the hybrid AC/DC microgrid which has energy storages on both AC side and DC side. A model of BPC has been built to design the inner loop and outer loop control strategy. The inner loop introduces the 0-axis control to suppress circulating current among the BPCs. The outer loop control proposes

a nine-quadrant control method to coordinate the SOCs of storages on both AC side and DC side. To ensure the output of storages do not exceed the maximum, a power limit loop was designed for BPCs.

With this strategy, the hybrid AC/DC system can achieve the mode switching and can realize AC subgrid and DC subgrid operating independently in the islanded mode. Since the method is a distributed control strategy, it can reduce the cost of communication and operation, and also manage the storages operating in a good state as much as possible. The effectiveness of the proposed strategy are verified by real-time hardware-in-loop tests.

Acknowledgments: This work is supported by National Key Research and Development Program of China (2016YFB0900500), State Grid Science and Technology Program (SGBJDK00DWJS 1700158), and Key Research and Development Plan of Zhejiang Province (2017C01039).

Author Contributions: All authors contributed equally in the presented research, and all authors approved the final manuscript.

Conflicts of Interest: The authors declare no conflicts of interest.

Abbreviations

The following abbreviations are used in this manuscript:

SOC	State of Charge
AC	Alternating current
DC	Direct current
BPC	Bidirectional Power Converters
DG	Distributed generators
HIL	Hardware-in-loop
PV	Photovoltaic

References

- Meng, L.; Shafiee, Q.; Trecate, G.F.; Karimi, H.; Fulwani, D.; Lu, X.; Guerrero, J.M. Review on Control of DC Microgrids and Multiple Microgrid Clusters. *IEEE J. Emerg. Sel. Top. Power Electron.* **2017**, *5*, 928–948.
- Xie, B.; Liu, Y.; Ji, Y.; Wang, J. Two-Stage Battery Energy Storage System (BESS) in AC Microgrids with Balanced State-of-Charge and Guaranteed Small-Signal Stability. *Energies* **2018**, *11*, 322. [[CrossRef](#)]
- Chen, X.; Hou, Y.; Hui, S.Y.R. Distributed Control of Multiple Electric Springs for Voltage Control in Microgrid. *IEEE Trans. Smart Grid* **2017**, *8*, 1350–1359. [[CrossRef](#)]
- Cagnano, A.; Tuglie, E.D.; Cicognani, L. Prince—Electrical Energy Systems Lab. *Elect. Power Syst. Res.* **2017**, *148*, 10–17. [[CrossRef](#)]
- Cagnano, A.; Tuglie, E.D. A decentralized voltage controller involving PV generators based on Lyapunov theory. *Renew. Energy* **2016**, *86*, 664–674. [[CrossRef](#)]
- Cagnano, A.; Bugliari, A.C.; Tuglie, E.D. A cooperative control for the reserve management of isolated microgrids. *Appl. Energy* **2018**, *218*, 256–265. [[CrossRef](#)]
- Yang, P.; Xia, Y.; Yu, M.; Wei, W.; Peng, Y. A Decentralized Coordination Control Method for Parallel Bidirectional Power Converters in a Hybrid AC/DC Microgrid. *IEEE Trans. Ind. Electron.* **2018**, *65*, 6217–6228. [[CrossRef](#)]
- Aryani, D.R.; Kim, J.S.; Song, H. Interlink Converter with Linear Quadratic Regulator Based Current Control for Hybrid AC/DC Microgrid. *Energies* **2017**, *10*, 1799. [[CrossRef](#)]
- Hu, W.; Chen, H.; Yang, X.; Xu, K.; Hu, P. Control strategy of the bi-directional converter for hybrid AC/DC microgrid. In Proceedings of the Power and Energy Engineering Conference, Brisbane, Australia, 15–18 November 2015; pp. 1–5.
- Sun, K.; Wang, X.; Li, Y.W.; Nejabatkhah, F.; Mei, Y.; Lu, X. Parallel Operation of Bidirectional Interfacing Converters in a Hybrid AC/DC Microgrid Under Unbalanced Grid Voltage Conditions. *IEEE Trans. Power Electron.* **2016**, *32*, 1872–1884. [[CrossRef](#)]
- Lu, X.; Guerrero, J.M.; Sun, K.; Vasquez, J.C.; Teodorescu, R.; Huang, L. Hierarchical Control of Parallel AC–DC Converter Interfaces for Hybrid Microgrids. *IEEE Trans. Smart Grid* **2014**, *5*, 683–692. [[CrossRef](#)]

12. Wang, P.; Jin, C.; Zhu, D.; Tang, Y.; Loh, P.C.; Choo, F.H. Distributed Control for Autonomous Operation of a Three-Port AC/DC/DS Hybrid Microgrid. *IEEE Trans. Ind. Electron.* **2015**, *62*, 1279–1290. [[CrossRef](#)]
13. Xiao, H.; Luo, A.; Shuai, Z.; Jin, G.; Huang, Y. An Improved Control Method for Multiple Bidirectional Power Converters in Hybrid AC/DC Microgrid. *IEEE Trans. Smart Grid* **2015**, *7*, 340–347. [[CrossRef](#)]
14. Loh, P.C.; Li, D.; Chai, Y.K.; Blaabjerg, F. Autonomous Operation of Hybrid Microgrid with AC and DC Subgrids. *IEEE Trans. Power Electron.* **2013**, *28*, 2214–2223. [[CrossRef](#)]
15. Eghtedarpour, N.; Farjah, E. Power Control and Management in a Hybrid AC/DC Microgrid. *IEEE Trans. Smart Grid* **2014**, *5*, 1494–1505. [[CrossRef](#)]
16. Loh, P.C.; Li, D.; Chai, Y.K.; Blaabjerg, F. Autonomous Control of Interlinking Converter with Energy Storage in Hybrid AC–DC Microgrid. *IEEE Trans. Ind. Appl.* **2013**, *49*, 1374–1382. [[CrossRef](#)]
17. Gu, Y.; Xiang, X.; Li, W.; He, X. Mode-Adaptive Decentralized Control for Renewable DC Microgrid with Enhanced Reliability and Flexibility. *IEEE Trans. Power Electron.* **2014**, *29*, 5072–5080. [[CrossRef](#)]
18. Sun, K.; Zhang, L.; Xing, Y.; Guerrero, J.M. A Distributed Control Strategy Based on DC Bus Signaling for Modular Photovoltaic Generation Systems with Battery Energy Storage. *IEEE Trans. Power Electron.* **2011**, *26*, 3032–3045. [[CrossRef](#)]
19. Wu, D.; Tang, F.; Dragicevic, T.; Guerrero, J.M.; Vasquez, J.C. Coordinated Control Based on Bus-Signaling and Virtual Inertia for Islanded DC Microgrids. *IEEE Trans. Smart Grid* **2015**, *6*, 2627–2638. [[CrossRef](#)]
20. Lu, X.; Sun, K.; Guerrero, J.M.; Vasquez, J.C.; Huang, L. State-of-Charge Balance Using Adaptive Droop Control for Distributed Energy Storage Systems in DC Microgrid Applications. *IEEE Trans. Ind. Electron.* **2014**, *61*, 2804–2815. [[CrossRef](#)]
21. Lu, X.; Sun, K.; Guerrero, J.M.; Vasquez, J.C.; Huang, L. Double-Quadrant State-of-Charge-Based Droop Control Method for Distributed Energy Storage Systems in Autonomous DC Microgrids. *IEEE Trans. Smart Grid* **2014**, *6*, 147–157. [[CrossRef](#)]
22. Karimi, Y.; Oraee, H.; Golsorkhi, M.S.; Guerrero, J.M. Decentralized Method for Load Sharing and Power Management in a PV/Battery Hybrid Source Islanded Microgrid. *IEEE Trans. Power Electron.* **2017**, *32*, 3525–3535. [[CrossRef](#)]
23. Hosseinzadeh, M.; Salmasi, F.R. Power management of an isolated hybrid AC/DC micro-grid with fuzzy control of battery banks. *Renew. Power Gener. IET* **2015**, *9*, 484–493. [[CrossRef](#)]
24. Xia, Y.; Peng, Y.; Yang, P.; Yu, M.; Wei, W. Distributed Coordination Control for Multiple Bidirectional Power Converters in a Hybrid AC/DC Microgrid. *IEEE Trans. Power Electron.* **2017**, *32*, 4949–4959. [[CrossRef](#)]
25. Xia, Y.; Li, Y.; Peng, Y.; Yu, M.; Wei, W. Circulating Currents Suppression Based on Two Degrees of Freedom Control in DC Distribution Networks. *IEEE Trans. Power Electron.* **2017**, in press. [[CrossRef](#)]
26. Xia, Y.; Yu, M.; Peng, Y.; Wei, W. Modeling and Analysis of Circulating Currents among Input-Parallel Output-Parallel Non-isolated Converters. *IEEE Trans. Power Electron.* **2017**, in press. [[CrossRef](#)]
27. Xia, B.; Lao, Z.; Zhang, R.; Tian, Y.; Chen, G.; Sun, Z.; Wang, W.; Sun, W.; Lai, Y.; Wang, M. Online Parameter Identification and State of Charge Estimation of Lithium-Ion Batteries Based on Forgetting Factor Recursive Least Squares and Nonlinear Kalman Filter. *Energies* **2017**, *11*, 3. [[CrossRef](#)]
28. Cui, X.; Jing, Z.; Luo, M.; Guo, Y.; Qiao, H. A New Method for State of Charge Estimation of Lithium-Ion Batteries Using Square Root Cubature Kalman Filter. *Energies* **2018**, *11*, 209. [[CrossRef](#)]
29. Dişçi, F.N.; El-Kahlout, Y.; Balıkcı, A. Li-ion battery modeling and SOC estimation using extended Kalman filter. In Proceedings of the 2017 10th International Conference on Electrical and Electronics Engineering (ELECO), Bursa, Turkey, 30 November–2 December 2017; pp. 166–169.
30. Lin, X. Theoretical Analysis of Battery SOC Estimation Errors under Sensor Bias and Variance. *IEEE Trans. Ind. Electron.* **2018**, in press. [[CrossRef](#)]
31. Meng, J.; Ricco, M.; Luo, G.; Swierczynski, M.; Stroe, D.I.; Stroe, A.I.; Teodorescu, R. An Overview and Comparison of Online Implementable SOC Estimation Methods for Lithium-ion Battery. *IEEE Trans. Ind. Appl.* **2018**, *54*, 1583–1591. [[CrossRef](#)]

